Presented at IPC SMEMA Council APEX® 2003
www.GoAPEX.org

HDPUG's Design for Lead-Free Solder Joint Reliability of High-Density Packages

John Lau
Agilent
Santa Clara, CA

Walter Dauksher
Agilent
Fort Collins, CO

Joe Smetana
Alcatel
Plano, TX

Rob Horsley
Celestica
Kidsgrove, UK

Dongkai Shangguan
Flextronics
San Jose, CA

Todd Castello
Flextronics
Youngsville, NC

Dave Love
Sun Microsystems
Menlo Park, CA

Bob Sullivan
HDPUG
Scottsdale, AZ

Irv Menis
IBM
Endicott, NY

Abstract
The lead-free solder-joint reliability of the high-density packages, 256-pin PBGA (plastic ball grid array), 388-pin PBGA, and 1657-pin CCGA (ceramic column grid array), on PCB (printed circuit board) subjected to temperature cycling is investigated. Emphasis is placed on the determination of the creep responses (e.g., stress, strain, and strain energy density) of the lead-free solder joints of these packages. The lead-free solder is assumed to obey the Garofalo-Arrhenius creep constitutive law. The results presented herein should be useful for a better understanding of the thermal-mechanical behaviors of the lead-free solder joints in these high-density package assemblies.

Introduction

Lead-Free Soldering

In the midnight of October 10, 2002, the EU Parliament and the EU Council of Ministers reached an agreement on a text for the WEEE (Waste Electrical and Electronic Equipment) and RoHS (Restriction of Hazardous Substances) directives. One of the items in the text is to ban Pb (lead) from July 1, 2006.

On October 11, 2002, the European Commission wasted no time and issued a high level Press Release to welcome the agreement made by the WEEE and RoHS. This means that from July 1, 2006, all the electronics products with leads (except those with exemptions listed in[1] cannot be produced in and shipped to all the EU Countries.

On February 13, 2003, the WEEE and RoHs were officially in forced. (This was published in the Official Journal of EU that day). All the Member States of the EU now have 18 months to put the Directives into their national legislation. In short, leadfree is now a law in EU.

What is a lead-free product? At present, there is no common world standard for lead-free products. However, the stipulation of the lead content as impurities to lead-free solders is recommended by JEDEC (Joint Electronic Device Engineering Conical) <0.2wt%Pb, JEIDA (Japanese Electronic Industry Development Association) <0.1wt%Pb, and EUELVD (EU End of Life Vehicles Directive) <0.1wt%Pb. Thus, lead-free products can be defined as those manufactured with the lead-free solders defined by either JEDEC or JEIDA and EUELVD, and those that don't allow any intentionally added Pb in the products. It should be pointed out and noted that solder joints with >85wt%Pb (e.g., the ceramic ball grid array, ceramic column grid array, and high-lead solder bumped flip chip) are exempted - this is, properly, the biggest joke of lead-free soldering!

What is the leading lead-free solder candidate? Sn-Ag-Cu! In Japan, the JEIDA recommended 96.5wt%Sn-3wt%Ag-0.5wt%Cu; in EU, the European Consortium - BRITE-EURAM recommended 95.5wt%Sn-3.8wt%Ag-0.7wt%Cu; and in US, the NEMI (National Electronics Manufacturing Initiative) recommended 95.5wt%Sn-3.9wt%Ag-0.6wt%Cu for reflow soldering and 99.3Sn-0.7Cu for wave soldering. This is significant! Now, the electronics industry can build the infrastructure (around the Sn-Ag-Cu) and form a critical mass to move forward.

There are many lead-free issues. For examples:[2-5]

- Overall costs increase
- Impact of PCB finishes
- Impact of component finishes
- Backward in-compatibility
- Forward in-compatibility
- Component reliability
- PCB reliability
- Impact of multiple heat cycles
- Tin whisker (short) reliability risk
- Solder joint reliability - thermal

- Solder joint reliability - mechanical
- Solder joint reliability - Shock & Vibration
- Reliability tests and acceleration factors
- Electrochemical reliability
- Infrastructure

In this study, the focus is on lead-free solder joint reliability of high-density packages.

Reliability Engineering of Solder Joints

Figure 1 shows the concept of reliability engineering[6] of solder joints. It consists of three major tasks, namely, design for reliability (DFR), reliability testing and data analysis, and failure analysis. Usually, the procedure starts off with a design (or a few designs) of the solder joints with the given high-density package and the corresponding PCB, and demonstrates that the design (or one of the few) is electrically, thermally, and mechanically reliable by analyses, e.g., the finite element method.

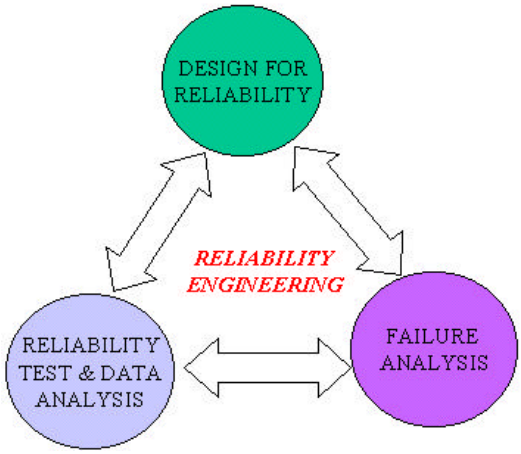

Figure 1 – The Reliability Engineering Concept

As a next step in the process, the "reliable" design is built with a certain sample size and these samples are tested under certain conditions. The objective of the test is to find failures (the more the better) and to choose a failure distribution (e.g., Weibull, lognormal, or exponential) to fit the failure data (to determine the parameters of the distribution). The distribution then becomes the life distribution of the solder joints.

Failure analysis should then be done on the failed samples in order to understand why they failed. This information is very useful for: (1) the next round of DFR and reliability testing and (2) choosing acceleration models to determine the acceleration factors since most of the reliability tests are naturally "accelerated." On the other hand, DFR will help failure analysis to find the (solder joint) failure locations. This study focuses on DFR. The reliability testing, data analysis, and failure analysis of high-density package lead-free solder joints are presented in References 7 and 8, respectively.

Objective

In this study, the reliability of lead-free solder joints of high-density packages such as the 256-pin and 388-pin PBGA (plastic ball grid array) and the 1657-pin CCGA (ceramic column grid array) is investigated. Emphasis is placed on the time-history creep responses such as the shear stress and shear creep strain hysteresis loops, shear stress history, shear creep strain history, and creep strain energy density of the lead-free solder joints of these packages on PCB while they are subjected to temperature cycling. The lead-free results will be compared to those with Sn-Pb solder joints.

Material Properties

The analysis correlates the solder joint fatigue life with the maximum creep energy density within select regions of the solder joint. Consequently, an accurate definition of the creep properties of the solders is an essential parameter in the analysis. Both the 95.5Sn-3.9Ag-0.6Cu and the Sn-Pb solders are assumed to follow the generalized Garofalo equation (sinh law), while the 10Sn-90Pb solder is modeled with the Norton equation (power law), as follows:[9]

$$\frac{\partial e}{\partial t} = C_1[\sinh(C_2 s)]^{C_3} \exp\left(\frac{-C_4}{T}\right)$$

$$\frac{\partial e}{\partial t} = C_1 s^{C_3} \exp\left(\frac{-C_4}{T}\right)$$

where the values of C_1 through C_4 are presented in Table 1. The experimental data presented in Figure 2 was used to derive the constants for the 95.5Sn-3.9Ag-0.6Cu.[10-11] The constants for the Sn-Pb are given in[12] and for the 10Sn-90Pb are given in.[6]

Table 1 – Creep Parameters

Solder alloy	C1 (1/sec)	C2 (1/Pa)	C3	C4 (°K)
95.5Sn-3.9Ag-0.6Cu	441000	5x10-9	4.2	5412
Sn-Pb	462(508 – T)/T	1/(37.78x106 - 74414T)	3.3	6360
10Sn-90Pb	$58.08/([1.732x10^{6}]^{C3})$	-	8.0696 - 0.0122T	7462

Note: All temperatures are in °K

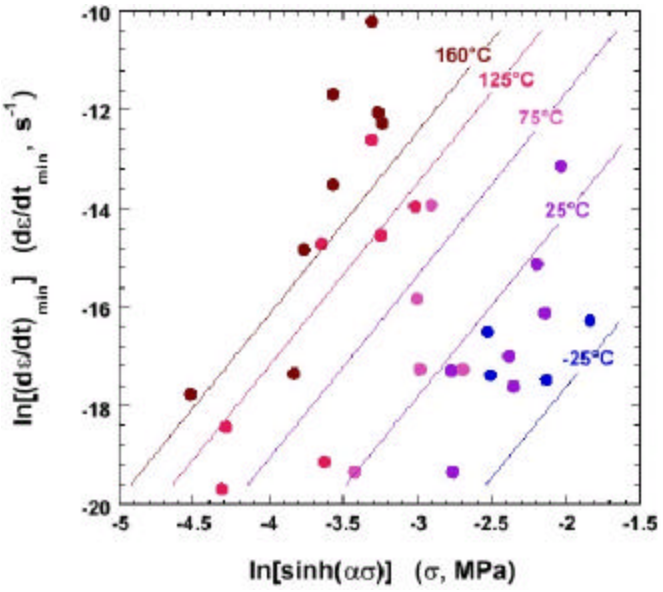

Figure 2 – 95.5Sn-3.9Ag-0.6Cu Creep Test Data – source: Sandia

Figures 3 through 5 detail the steady state creep rate for the solders at 0°C, 50°C and 100°C, respectively. It can be seen that the creep strain rate difference between the lead-free solder and the lead bearing solder is temperature dependent, and that the higher the temperatures the higher the creep strain rate differences. For the temperatures of 50°C or greater and for a given normal stress, the 95.5Sn-3.9Ag-0.6Cu solder has a creep rate that is one-half to two orders of magnitude lower than that of the lead bearing solders. Hence, significantly lower creep strains are expected with the 95.5Sn-3.9Ag-0.6Cu solder in comparison the leaded solders.

The remaining material properties are specified in Table 2. The elastic modulus and coefficient of thermal expansion for the 95.5Sn-3.9Ag-0.6Cu solder are derived from recent experimental data,[11] see Figure 6 and Figure 7.[6, 12]

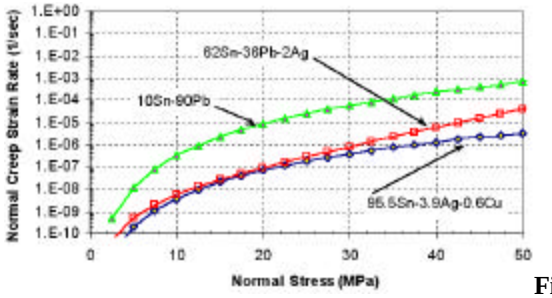

Figure 3 – Steady State Creep of Solders at 0°C

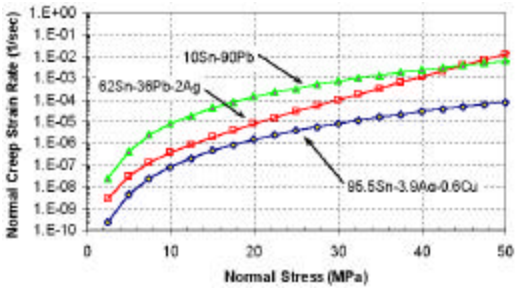

Figure 4 – Steady State Creep of Solders at 50°C

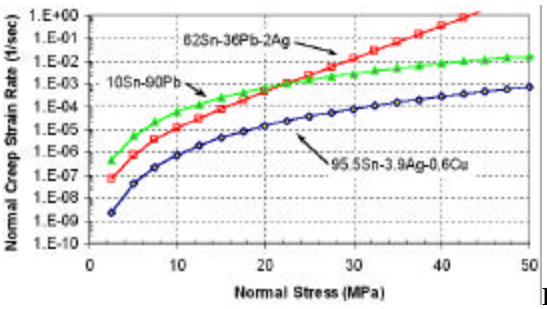

Figure 5 – Steady State Creep of Solders at 100°C

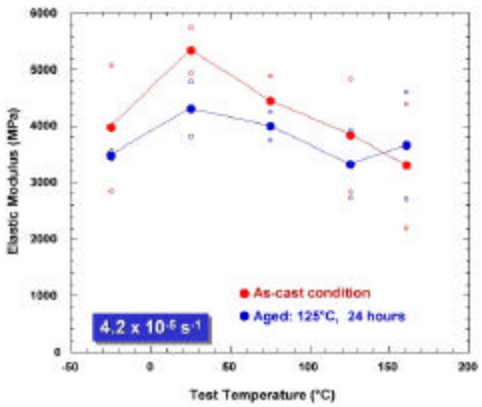

Figure 6 – Static Elastic Modulus of the 95.5Sn-3.9Ag-0.6Cu Solder Versus Temperature

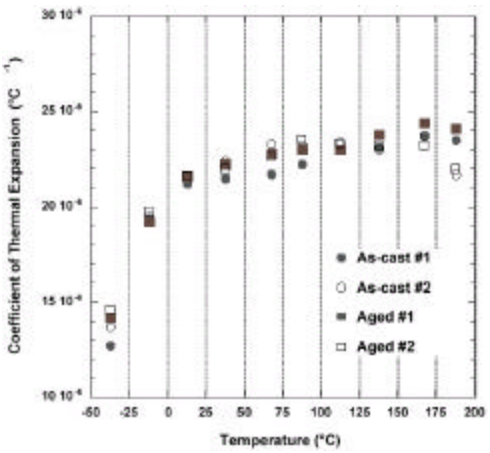

Figure 7 – Coefficient of Thermal Expansion of the 95.5Sn-3.9Ag-0.6Cu Solder Versus Temperature

Table 2 – Material Properties

Material	Young's modulus (GPa)	Poisson's ratio	CTE (ppm/°K)
PC board	27	0.39	18
Copper pad	76	0.35	17
95.5Sn-3.9Ag-0.6Cu	74.84 - 0.08T	0.3	16.66 + 0.017T
Sn-Pb	75.94 – 0.152T	0.35	24.5
10Sn-90Pb	23.71 – 0.047T	0.35	24.495 + 0.015T
Laminate substrate	Same as PC board		
Al_2O_3 substrate	270	0.3	5.5
Si	167	0.28	2.54
256 PBGA overmold	13	0.3	15
388 PBGA overmold	20	0.25	10
1657 CCGA lid	70	0.33	23
1657 CCGA lid seal	0.0024	0.35	270

Note: All temperatures are in °K

Creep Analysis of the CCGA1657 Assembly

The Structure

Finite element models were constructed for each of the studied packages. Except where noted, the modeling strategy and thermal environment discussed in detail for the CCGA packages also applies to the PBGA packages.

Since the time dependent analysis includes nonlinear material properties and since a significant quantity of results data were saved during the analyses, the finite element models were constructed such that an economy of elements were used overall. As shown in Figure 8, the package is modeled as a three-dimensional strip that captures the construction along a diagonal path from the package's geometric center to a corner. Due to the symmetry about the vertical midplane of a full strip and as shown in the figure, the models are actually half strips with the appropriate in-plane restraints placed on one symmetry plane. Coupled in-plane translations are applied to the other symmetry plane to produce a state of generalized plane strain. Using exclusively hexahedral solid elements, the models can capture the precise shape of the packages' solder columns and potential DNP (distant to neutral point) effects while

retaining significant computational efficiency over full octant models. ANSYS[13] was the code selected for the modeling and analyses.

Despite the overall economy of elements in each strip model, selective mesh refinement was used to concentrate highly refined elements in the solder joints where failure was anticipated. In the case of the CCGAs, failure would be predicted in the column with the greatest DNP and close to the intersection of the column with the vertex of the fillets.[14]

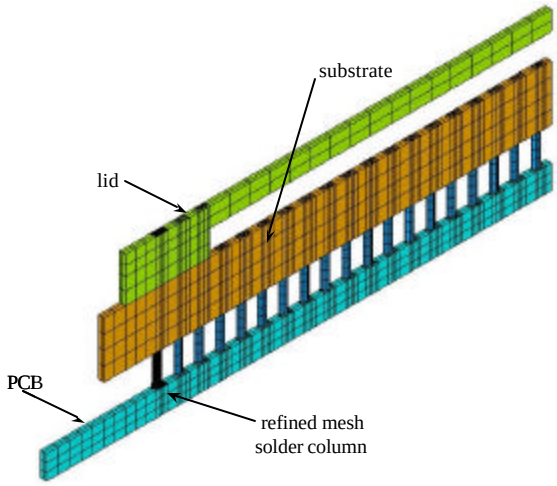

Figure 8 – The CCGA Model

There are two components to the selective refinement, the first being the refinement within a model of only the solder joint with anticipated first failure and the second being the use of graded meshes within this critical solder joint. Of the 16746 elements in the CCGA model shown in Figure 8, 6528 are used in the single refined solder column and fillets while each of the coarsely meshed solder columns are constructed with just 48 elements. In addition to the concentration of elements in the greatest DNP solder column, mesh grading refines the thickness of these elements toward the intersection of the column with each of the fillets. A detail of the refined mesh column is shown in Figure 9; the figure focuses on the PCB fillet. Such mesh grading increases the fidelity of the calculated stresses and strains while saving on element count. In all refined solder interconnects, the grading produces elements, used in results reporting, with a thickness of approximately 18µm. Since the thickness can impact the results calculation, a consistent thickness is required in order to compare results among models.

The CCGA's Al_2O_3 substrate measures 42.5x42.5x3.75mm and has a cavity lid with an edge length of 40.5mm and an overall thickness of 3mm. The actual thickness of the lid over the cavity ranges from 1.3 to 1.7mm; a 1.3mm thickness was used in the analyses. As shown in Figure 10, the 0.5mm diameter columns are modeled as 10Sn-90Pb and are 2.21mm tall. A fillet, assumed to be eutectic solder, attaches the column to the substrate.

The second-level columns form a 41x41 array at 1mm pitch with six pins depopulated per corner. This results in 1657 second-level pads. The finite element model includes 19 columns. The inner 18 columns are coarsely meshed while the outermost column is constructed with a highly refined mesh. While the pads on the 1.6mm thick PCB are 0.673mm in diameter, the diameter of those on the substrate is 0.8mm. Since the strip model for this package should be 0.707mm thick, incorporating the substrate pad necessitated a reasonable modification to the modeled geometry. The thickness of the strip was increased to 0.8mm while the substrate's pad diameter was set to 0.75mm.

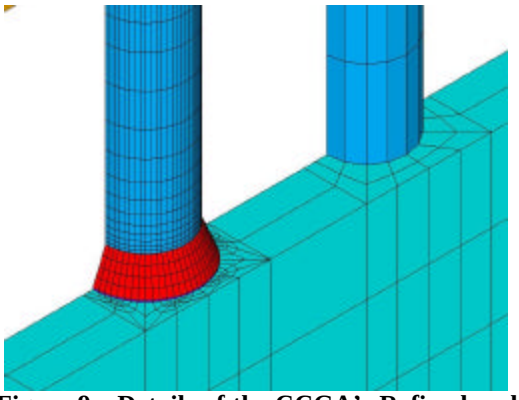

Figure 9 – Details of the CCGA's Refined and Coarse Columns Showing the PCB and Fillet

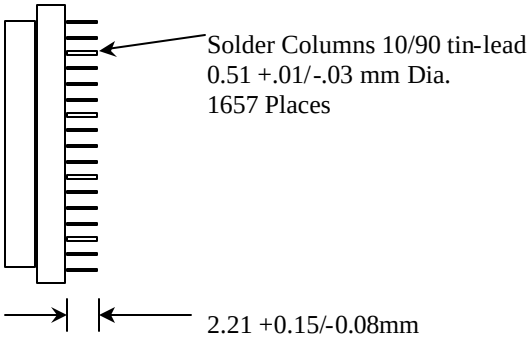

Figure 10 – A Notional View of the CCGA from the Side

Two models were developed for the CCGA package. In the first, Sn-Pb solder is used as the PCB attach fillet while in the second, 95.5Sn-3.9Ag-0.6Cu solder forms the PCB attach fillet. It should be emphasized that this difference should have minor impact on the nonlinear responses, since the failure mode is at the high-lead solder column.

Boundary Conditions

Temperature loads are applied to the models that represent the chamber cycling environment. After starting at room temperature, each model is subject of 5 cycles consisting of 10-minute ramps and 10-minute holds at each of 273°K and 373°K. Five cycles, as shown in Figure 11, are executed in order to confirm the stabilization of the creep responses.

Deformed Shape

The out-of-plane (vertical) displacement of the substrate's free end was examined as a metric for the package deformation. Since these packages differ only in the substrate fillet materials, there is no discernable difference in the out-of-plane displacements between the packages.

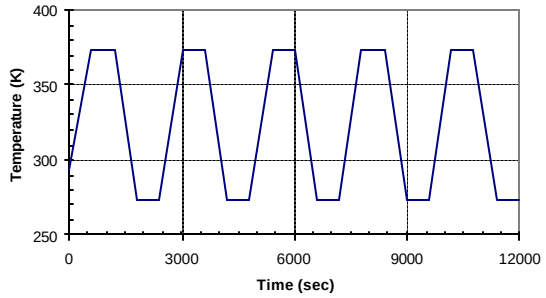

Figure 11 – The Thermal Environment Applied to the Models

Consequently, representative data is presented in Figure 12. From the figure, the deformation is in phase with the thermal profile. In addition, creep deformation is evident during the isothermal holds.

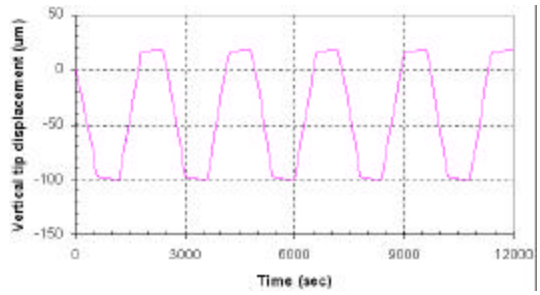

Figure 12 – Tip Displacement of the 1657 CCGA

Time-Dependent Shear Stress and Creep Shear Strain

As with the modeling strategy, a common methodology was used in both results reporting and in the prediction of the failure initiation site within the refined solder joint. Derived results, which include stresses, strains and energies, are examined within a number of elements in the refined solder joints and the highest values are presented and used in predicting failure locations. Reported stresses, strains and energies are nodal values rather than element-averaged results. To avoid well known averaging problems, results reporting is performed with only the solder material selected.

Failure in the CCGA packages is predicted to start in the high-lead solder column at the "vertex" of the substrate solder fillet and the PCB solder fillet. Cross sectioning of the temperature cycling failure sample, as shown in Figure 13, confirms this prediction in the CCGA packages.

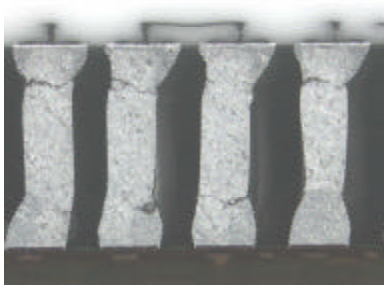

Figure 13 – Temperature Cycling Failures in the 1657 CCGA Solder Column

Representative plots of the shear stress and shear creep strains (in the direction of thermal expansion mismatch between the ceramic carrier and the PCB) within the columns at 9000 seconds are presented in Figures 14 through 17. In the figures, the location of the highest stresses and strains corresponds with the predicted failure sites.

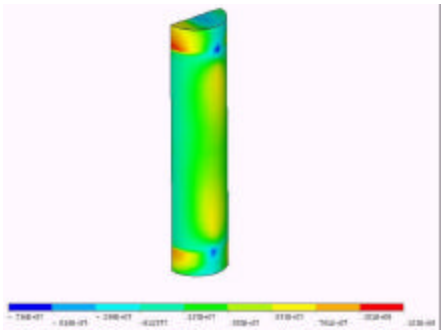

Figure 14 – Shear Stress (Pa) at 9000 Seconds in the 1657 CCGA's Refined-Mesh Column. A Sn-Pb Fillet is Used at the PCB.

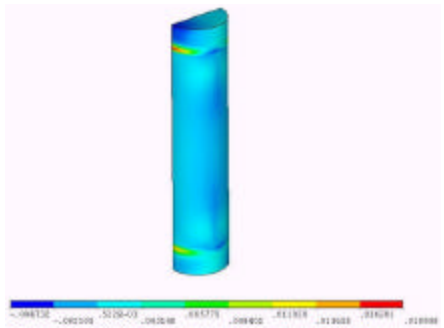

Figure 15 – Creep Shear Strain at 9000 Seconds in the 1657 CCGA's Refined-Mesh Column. A Sn-Pb Fillet is Used at the PCB.

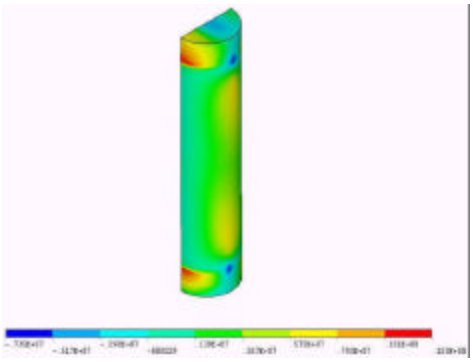

Figure 16 – Shear Stress (Pa) at 9000 Seconds in the 1657 CCGA's Refined-Mesh Column. A 9455.5Sn-3.9Ag-0.6Cu Fillet is Used at the PCB.

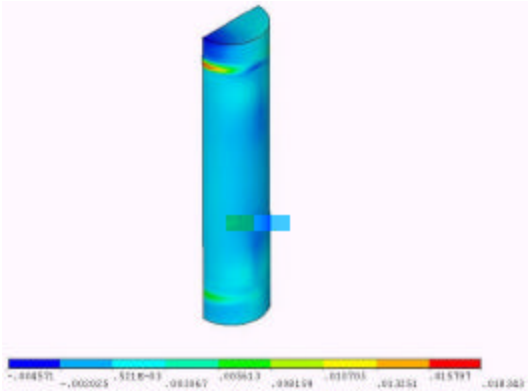

Figure 17 – Creep Shear Strain at 9000 Seconds in the 1657 CCGA's Refined-Mesh Column. A 95.5Sn-3.9Ag-0.6Cu Fillet is Used at the PCB.

The maximum shear stress and creep shear strain at the predicted failure site within the CCGA models are shown in Figure 18 and Figure 19. It can be seen that the maximum shear stress range and the maximum shear creep strain range in the high lead columns assembled with the lead-free solder paste (15MPa and 0.065) are larger than that with the Sn-Pb paste (12.5MPa and 0.051). However, all these values are within the reliable ranges for high-lead solder column in most of the applications.[6, 14]

Creep Hysteresis Loops

When the shear stresses are plotted as a function of the creep shear strain, the hysteresis present in each thermal cycle is obtained. The hysteresis within the CCGAs, presented in Figure 20, shows a stabilized response (the area under the shear stress and creep shear strain hysteresis loop) within the five cycles analyzed. Also, it can be seen that the area (creep strain energy density) under the lead-free hysteresis loop is larger than that under the Sn-Pb hysteresis loop. Thus, the thermal fatigue life for the high-lead solder columns with the Sn-Pb solder paste should be longer than that with the lead-free paste. This is due to the higher stiffness (Young's modulus) of the lead-free solder, which transmits greater stress to the high-lead column.

Creep Analysis of the PBGA256 Assembly

The Structure

Experience has shown that certain PBGA package-to-board solder interconnects are most likely to fail in 0°C to 100 °C part-on-board thermal cycling. Due to (1) the very high local thermal expansion mismatch between the die and the laminate substrate and (2) the relatively high die stiffness and the flexibility of the laminate substrate, the ball closest to the die shadow will likely fail first in PBGA packages.[15] As such, mesh refinement was deliberately applied to the solder ball that is predicted to fail first. Figure 21 presents the location of the refined solder ball for the 256 PBGA package. The 256 PBGA has a total of 6408 elements, of which 1920 are in the refined ball and 24 elements are used in each of the coarsely meshed balls.

Failures are assumed, in the case of the PBGAs, to occur in the solder in the proximity of the pads. As shown in Figure 21, the elements in the solder balls are refined as they approach each of the substrate and PCB pads.

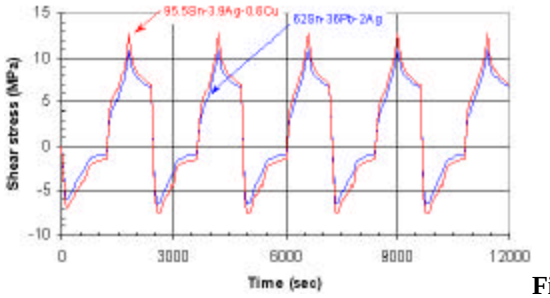

Figure 18 – Shear Stress Versus Time in the 1657 CCGAs' Refined-Mesh Column

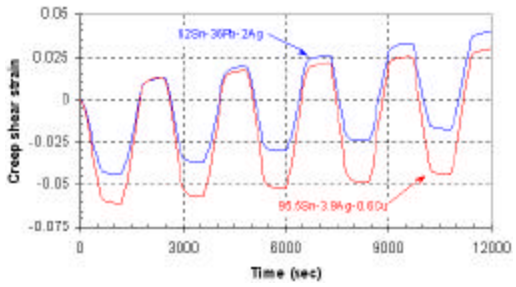

Figure 19 – Creep Shear Strain Versus Time in the 1657 CCGAs' Refined-Mesh Columns

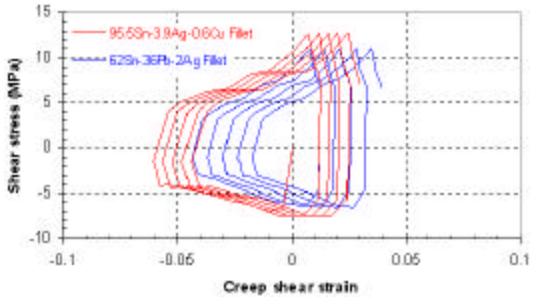

Figure 20 – Hysteresis in the 1657 CCGAs' Refined-Mesh Columns

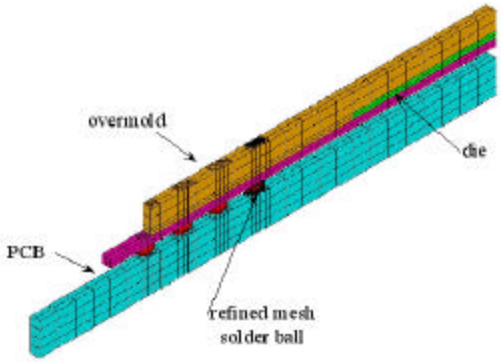

Figure 21 – The 256 PBGA Model

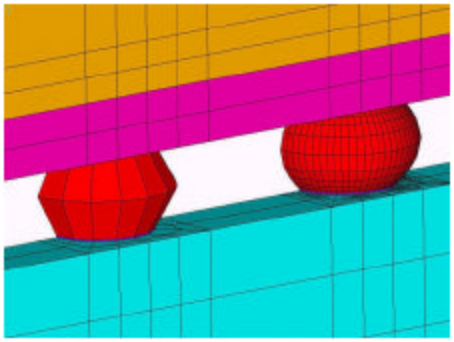

Figure 22 – Details of the Refined and Coarse Ball Meshes in the PBGA Packages

The 256 PBGA has a 27x27x0.36mm substrate with a 10x10x0.3mm die and 1.17mm thick overmold. The package has 0.635mm diameter pads on the substrate and the assembled ball is assumed to have a height of 0.5mm and a maximum diameter of 0.9mm. Ball pitch is 1.27mm for the PBGA packages. Additionally, the PCB thickness is 1.6mm and the pad diameter is 0.635mm.

Two models are constructed. In the first, both the solder ball and the paste are Sn-Pb solder. The second model examines the case of 95.5Sn-3.9Ag-0.6Cu solder balls and paste.

Boundary Conditions

The thermal loads applied to the 1657 CCGA are also applied to the 256 PGBA. This thermal profile is shown in Figure 11.

Deformed Shape

The vertical displacements of the free edge of the 256 PBGA models' substrate are presented in Figure 23. From the figure, the reported deflections are in phase with the applied temperature profile. The peak-to-peak displacement appears to be largely unaffected by the local solder ball material.

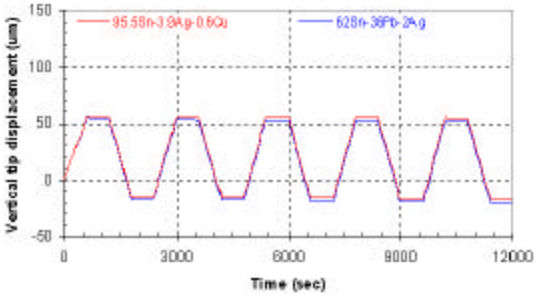

Figure 23 – Vertical Displacement of the 256 PBGA Package Tip

Time-Dependent Shear Stress

The 256 PBGA models predict that failures are likely to occur in the solder ball near the PCB pads and the package substrate pads, since the creep responses (stress, creep strain and creep strain energy) at these locations are very similar. Figures 24 and 25 present the von-Mises stress in the two solder balls at 9000 seconds. It can be seen that, for both solders, the maximum stress occurs at the interface near the package substrate pad and the PCB pad. Also, the maximum von-Mises stress in the lead-free solder joint is more than 10% higher than that in the tin-lead solder joint.

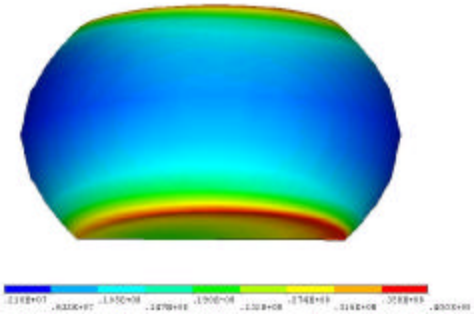

Figure 24 – Von-Mises Stress (Pa) at 9000 Seconds in the 256 PBGA's Refined Sn-Pb Solder Ball

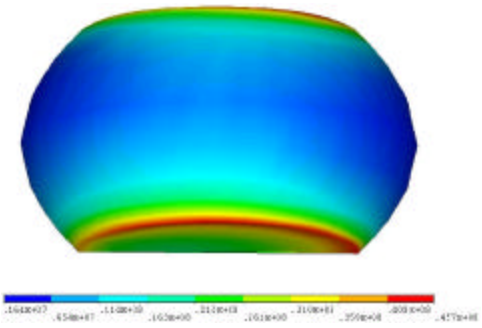

Figure 25 – Von-Mises Stress (Pa) at 9000 Seconds in the 256 PBGA's Refined 95.5Sn-3.9Ag-0.6Cu Solder Ball

Figure 26 depicts the complete shear stress-time history at the predicted solder fatigue failure initiation sites for the 256 PBGA packages. The stresses within 95.5Sn-3.9Ag-0.6Cu solder exceed those in the Sn-Pb solder. As evidenced by Figure 23, the general deformation of this package is not significantly affected by the solder interconnect material. Consequently, it may be presumed that the solder interconnect is subject to displacement controlled loading. Then, the higher stiffness (Young's modulus) of the 95.5Sn-3.9Ag-0.6Cu solder would result in stresses greater then those in the Sn-Pb solder.

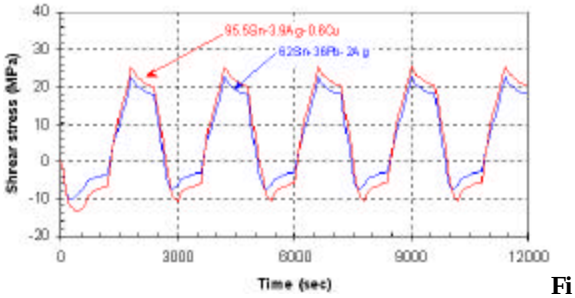

Figure 26 – Shear Stress Versus Time in the 256 PBGA

Time-Dependent Creep Shear Strain

Snap shots of the von-Mises (effective) creep strains at 9000 seconds are presented for the Sn-Pb and 95.5Sn-3.9Ag-0.6Cu solders in Figure 27 and Figure 28, respectively. Again, it can be seen that, for both solders, the maximum creep strains occur near the upper and the lower interfaces of the solder joint. The corresponding maximum creep shear strains through the 12000-second analysis are presented in Figure 29. The figures show that, as expected from Figure 3 through 5, the creep shear strain is lower in the 95.5Sn-3.9Ag-0.6Cu solder when compared to that in the Sn-Pb solder.

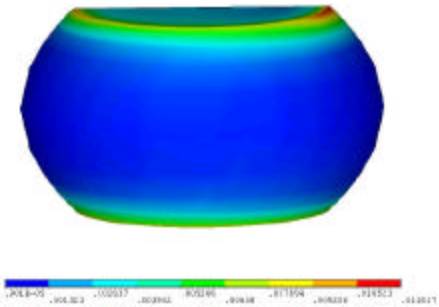

Figure 27 – Von-Mises Creep Strain at 9000 Seconds in the 256 PBGA's Refined Sn-Pb Solder Ball

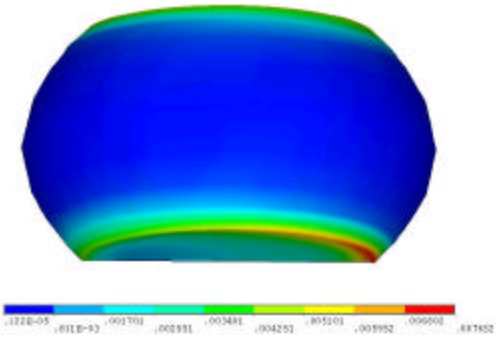

Figure 28 – Von-Mises Creep Strain at 9000 Seconds in the 256 PBGA's Refined 95.5Sn-3.9Ag-0.6Cu Solder Ball

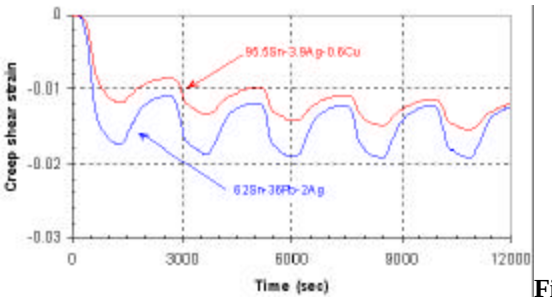

Figure 29 – Creep Shear Strain Versus Time in the 256 PBGA

Creep Hysteresis Loops

Figure 30 presents the hysteresis in the 256 PBGA packages. The hysteresis loops indicate that a stabilized response is obtained within the five cycles examined. Reflecting the material's greater stiffness and lower propensity toward creep deformation, the 95.5Sn-3.9Ag-0.6Cu solder's hysteresis loops are both taller and narrower than those of the Sn-Pb solder. Also, it can be seen that the area under the hysteresis loops (creep strain energy) for the lead-free solder joint is smaller than that for the tin-lead solder joint.

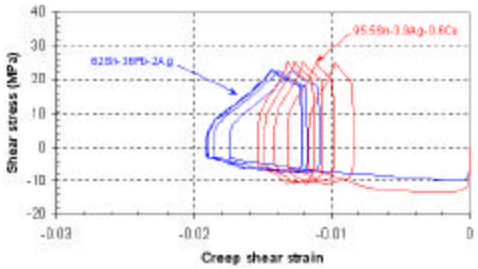

Figure 30 – Hysteresis in the 256 PBGA

Creep Analysis of the PBGA388 Assembly

The Structure

The 388 PBGA substrate's dimensions are 35x35x0.56mm and the package has an 8.4x8.4x0.3mm die and 1.17mm thick overmold. Both the substrate and the PCB have 0.635mm diameter pads and the assembled ball is assumed to have a height of 0.5mm and a maximum diameter of

0.9mm. The ball pitch, as shown by Figure 31, is 1.27mm for the 388 PBGA packages. Again, the PCB thickness is 1.6mm. Due to the thermal expansion mismatch and the stiffness effects associated with the die and the laminate substrate, first failure is expected to occur in the outermost row of the inner ball array.

The finite element strip model is shown in Figure 32. Using the refinement methodology previously discussed, the model has only 7396 elements. Of these, 1920 are in the refined solder ball where first failure is expected. As for the 256 PBGA, two models are constructed. The first considers Sn-Pb solder spheres with Sn-Pb solder paste. The second model examines 95.5Sn-3.9Ag-0.6Cu solder balls and paste.

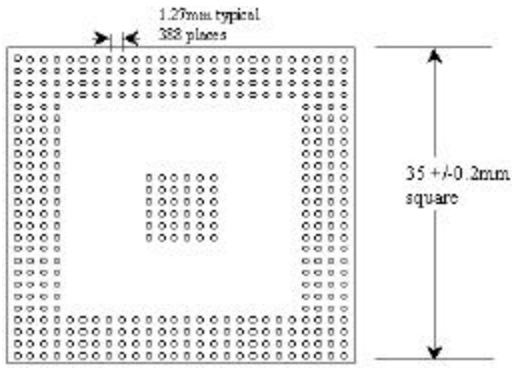

Figure 31 – The Second-Level Pads for the 388 PGBA

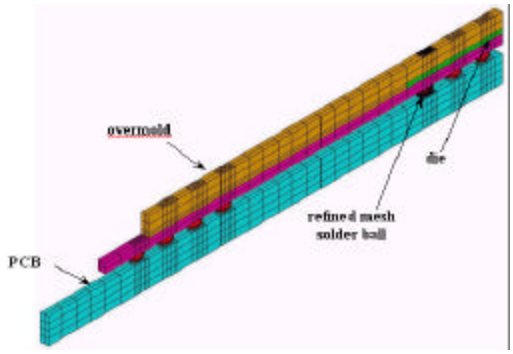

Figure 32 – The 388 PBGA Model

Boundary Conditions

The thermal loads applied to the 1657 CCGA are also applied to the 388 PGBA. This thermal profile is shown in Figure 11.

Deformed Shape

The substrates' out-of-plane deflections, taken as a metric for the packages' thermal responses, are presented in Figure 33. As for the 256 PBGA, there is no significant difference in the peak-to-peak displacement due to the solder material. In addition, the deflection of the 388 PBGA is significantly higher than that of the 256 PBGA as shown in Figure 23. This difference is likely attributed to the 388 PBGA's greater package size. Considering either package, the displacement's amplitude appears to be largely unaffected by the local solder ball material.

Time-Dependent Shear Stress

The models predict that failure is likely to occur in the solder ball near the substrate pad and the PCB pad for the 388 PBGAs. This is evident by viewing Figures 33-35 for the von-Mises stress distribution in the Sn-Pb and 95-5Sn-3.9Ag-0.6Cu balls, respectively, at 9000 seconds. The complete shear stress versus time history is presented in Figure 36. Again, stresses are greater in the stiffer (Table 2) 95-5Sn-3.9Ag-0.6Cu solder joints.

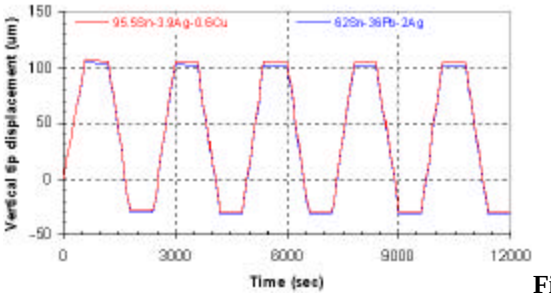

Figure 33 – Vertical Displacement of the 388 PBGA Package Tip

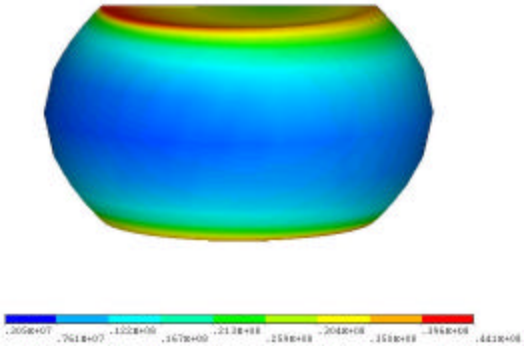

Figure 34 – Von-Mises Stress (Pa) at 9000 Seconds in the 388 PBGA's Refined Sn-Pb Solder Ball

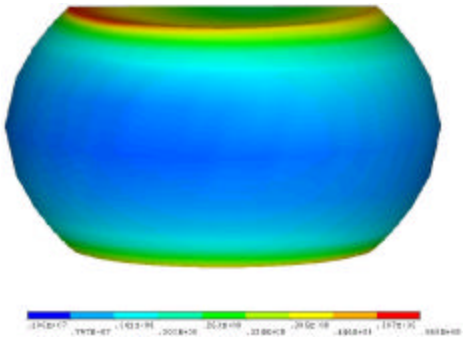

Figure 35 – Von-Mises Stress (Pa) at 9000 Seconds in the 388 PBGA's Refined 95.5Sn-3.9Ag-0.6Cu Solder Ball. Note that the Maximum Value at this Time Occurs on the Substrate Side

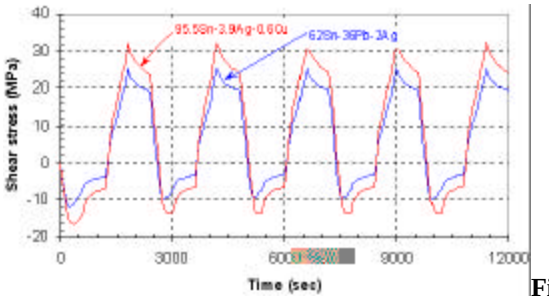

Figure 36 – Shear Stress Versus Time in the 388 PBGA

Time-Dependent Creep Shear Strain

The von-Mises creep strain at 9000 seconds is shown in Figure 37 and Figure 38 for the two solders examined. It can be seen that the maximum effective creep strain, for both solders, occurs near the interface of the package substrate pads and the PCB pads. Thus, these locations are the most likely cracking paths of the 388-pin PBGA lead-free and tin-lead solder joints.

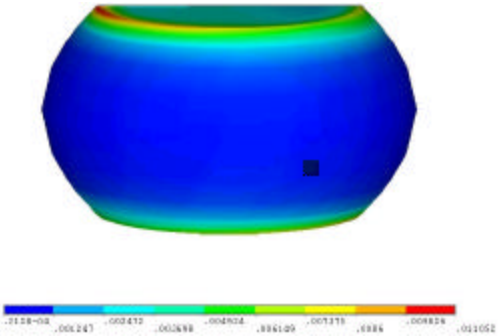

Figure 37 – Von-Mises Creep Strain at 9000 Seconds in the 388 PBGA's Refined Sn-Pb Solder Ball

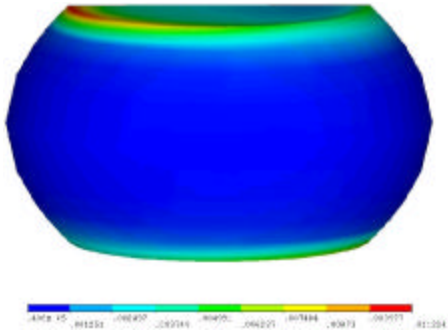

Figure 38 – Von-Mises Creep Strain at 9000 Seconds in the 388 PBGA's Refined 95.5Sn-3.9Ag-0.6Cu Solder Ball

Figure 39 depicts the complete shear creep strain history. As seen previously and as explained by the creep constitutive properties, lower creep shear strains are seen in the 95-5Sn-3.9Ag-0.6Cu solder than in the Sn-Pb solder.

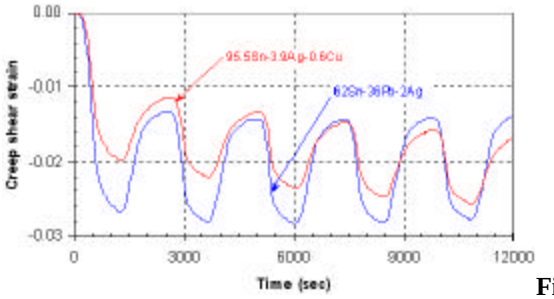

Figure 39 – Creep Shear Strain Versus Time in the 388 PBGA

Creep Hysteresis Loops

Figure 40 presents the shear stress versus creep shear strain throughout the analysis. From the figure, there is a stable hysteresis response developed during the coarse of the analysis. Again, the creep strain energy (the area under the shear stress and shear creep strain hysteresis loop) in the tin-lead solder joint is larger than that in the lead-free solder joint.

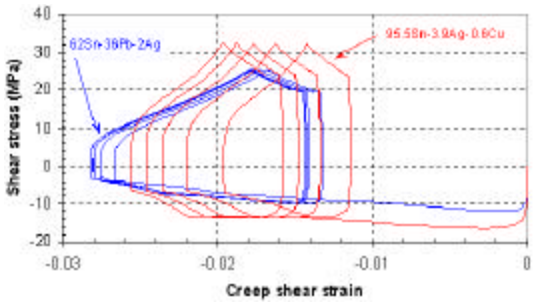

Figure 40 – Hysteresis in the 388 PBGA

Thermal Fatigue Life of Solder Joints

Thermal fatigue life of solder joints (dominated by creep responses) may be predicted by the following equation[16]

$$N_f = a(\Delta W)^b$$

where N_f is the number of cycle to failure, $?W$ is the creep strain energy density per cycle, and a (always positive) and $ß$ (always negative) are material constants for the solder joints. In this equation, a and $ß$ are usually determined by isothermal fatigue tests of the solder-joint material and $?W$ can be determined by creep analysis of the structure (package, solder joints, and PCB) subjected to loading conditions. Since the material constants for the 95-5Sn-3.9Ag-0.6Cu lead-free solder are not available at the time of this writing, thermal fatigue life prediction of the lead-free solder joints is impossible. However, with the calculated creep strain energy density per thermal cycle (the area under the creep hysteresis loop), the above equation may lead us to some useful insights of the lead-free solder-joint reliability of the three packages considered.

For the PBGA packages, the von-Mises creep strain energy densities (*W*) at the predicted failure initiation sites are presented in Figure 41. *?W* is determined as the change in the value of *W* over a cycle. *?W* is approximately 0.112 MPa and 0.160 MPa for the 256 PBGA with 95.5Sn-3.9Ag-0.6Cu and Sn-Pb solder joints, respectively. Without the fatigue constants α and β, the absolute life prediction for these two solders is impossible. However, if we assume that α and β are the same (which is unlikely) for both the tin-lead and the lead-free solders, then the thermal fatigue life of the lead-free solder is greater than that of the tin-lead solder.

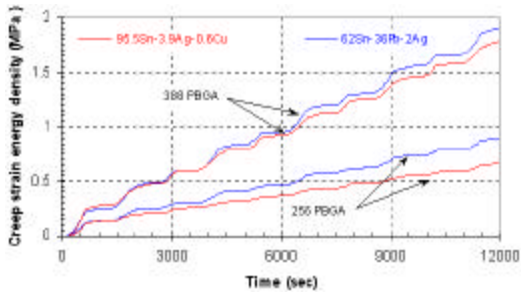

Figure 41 – Creep Strain Energy Density for the PBGA Packages

For the 388 PBGAs, the stabilized values of *?W* are much closer with a value of 0.327 MPa for the 95.5Sn-3.9Ag-0.6Cu solder joints and 0.353 MPa for the Sn-Pb solder joints. Again making the assumption that the fatigue constants are the same for both solder alloys, the thermal fatigue life of the lead-free solder joint is slightly better than that of the tin-lead solder joint.

For both lead-free and tin-lead solder joints, the creep strain energy density in the 388-pin PBGA is larger than that in the 256-pin PBGA. Thus, as expected, the thermal fatigue life of the 256-pin PBGA solder joints should be longer than that of the 388-pin PBGA.

The von-Mises creep strain energy density associated with failure in the CCGA packages is presented in Figure 42. It can be seen that *?W* in the high-lead solder column with the lead-free paste is larger than that with the Sn-Pb paste. Thus, the high-lead columns with the Sn-Pb paste should have a longer thermal fatigue life than those with the lead-free solder paste.

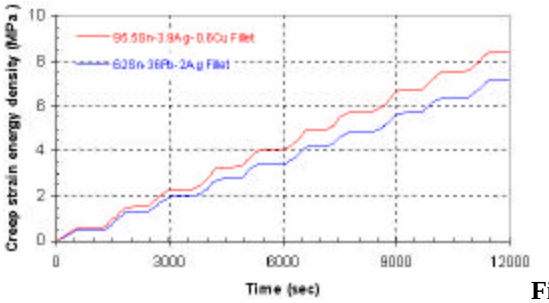

Figure 42 – Creep Strain Energy Density for the 1657 CCGA

Summary and Recommendations

Nonlinear 3D temperature-dependent and time-history analyses of high-density packages (PBGAs and CCGAs) on PCB subjected to temperature cycling have been presented. The deflection, creep hysteresis loops, stress time-history, creep strain time-history, and the creep strain energy density time-history of the lead-free solder joints of these packages have also been provided for a better understanding of their thermal-mechanical behaviors. Some important results are summarized in the following:

- The Young's modulus of the lead-free solder is larger than that of the tin-lead solder. Thus, in general, higher stresses should be expected in the lead-free solder joints.
- The creep strain rate of the lead-free solder is less than that of the tin-lead solder, especially at higher temperatures. Thus, in general, lower creep strains should be expected in the lead-free solder joints.
- The predicted failure locations (at the high-lead column near the "vertex" of the substrate solder fillet and the PCB solder fillet) of the CCGA compared very well with the temperature cycling results.[7, 8]
- The creep responses of the CCGA (stress, strain, and creep strain energy density) at the failure locations are higher with the lead-free solder fillets. Thus, the thermal-fatigue life of the high-lead columns is longer with the Sn-Pb solder fillets.
- The creep responses of the CCGAs with both lead-free and Sn-Pb solder fillets are within the reliable ranges for most of the applications.
- The predicted failure locations of the 256-pin and 388-pin PBGAs are near the interface of the package substrate pads and the near the interface of PCB pads, which compared very well with the test results reported in the literature.
- For both the 256-pin and 388-pin PBGAs, the shear stress in the lead-free solder joints is higher than that in the tin-lead solder joints.

- For both the 256-pin and 388-pin PBGAs, the shear creep strain in the lead-free solder joints is lower than that in the tin-lead solder joints.
- For both the 256-pin and 388-pin PBGAs, the creep strain energy (the area under the creep hysteresis loop) in the lead-free solder joints is lower than that in the tin-lead solder joints. Consequently, the thermal-fatigue life of the lead-free solder joints is expected to be longer than that of the tin-lead solder joints. Again, this is based on the assumption that the material constants (α and β) are the same for the lead-free and the tin-lead solders.
- For either lead-free or tin-lead solder joints, the creep strain energy density of the 388-pin PBGA is larger than that of the 256-pin PBGA. Thus, as expected, the thermal-fatigue life of the smaller package (225-pin) is longer than that of the larger package (338-pin).
- The fatigue crack-growth material constants (α and β) for the lead free solder are desperately needed in order to make quantitative solder-joint thermal-fatigue life predictions.

Acknowledgements

The authors of this paper would like to acknowledge and thank the many unnamed contributors from the various companies that made this test program possible. These include, but are probably not limited to, contributions from unnamed people at, or formerly employed at, Agilent, Alcatel, Amkor, Celestica, ChipPac, Fairchild Semiconductor, Flextronics, HDPUG, Hewlett Packard Co., IBM, International Tin Research Institute, Lucent, National Semiconductor, Nokia, Nortel Networks, RF Monolithics, ST Microelectronics, Sun Microsystems, Texas Instruments, and Thomas and Betts. Special thanks to Paul Vianco of Sandia for providing the constitutive equation of the lead-free solder, to Marie Cole of IBM for her useful inputs on the CCGA package, and to Ruben Bergman of HDPUG, Ted Lancaster and Pete Woodhouse of Agilent for their strong support of this project.

References

1. Smetana, J., R. Horsley, J. Lau, K. Snowdon, D. Shangguan, J. Gleason, I. Memis, D. Love, W. Dauksher, and B. Sullivan, "Lead-Free Design, Materials, and Process of High Density Packages", *Proceedings of APEX*, Anaheim, CA, CD-ROM, March 2003.
2. Hwang, J. S., *Environmentally Friendly Electronic Lead-Free Technology*, Electrochemical Publications, Ayr, Scotland, 2001.
3. Lau J. H., C. P. Wong, N. C. Lee, and R. Lee, *Electronics Manufacturing with Lead-Free, Halogen-Free, and Conductive Adhesive Materials*, McGraw-Hill Book Company, New York, NY, 2002.
4. Lau, J. H., R. Lee, *Microvias for Low Cost, High Density Interconnects*, McGraw-Hill Book Company, New York, NY, 2001.
5. Lau, J. H., Low Cost Flip Chip Technologies for DCA, WLCSP, and PBGA Assemblies, McGraw-Hill Book Company, New York, NY, 2000.
6. Lau, J. H., and Y. Pao, Solder Joint Reliability of BGA, CSP, Flip Chip, and Fine Pitch SMT Assemblies, McGraw-Hill Book Company, New York, NY, 1997.
7. Lau, J., N. Hoo, R. Horsley, J. Smetana, D. Shangguan, W. Dauksher, D. Love, I. Menis, and B. Sullivan, "Reliability Testing and Data Analysis of High-Density Packages' Lead-Free Solder Joints", *Proceedings of APEX*, Anaheim, CA, CD-ROM, March 2003.
8. Lau, J., D. Shangguan, T. Castello, R. Horsley, J. Smetana, W. Dauksher, D. Love, I. Menis, and B. Sullivan, "Failure Analysis of High-Density Packages' Lead-Free Solder Joints", *Proceedings of APEX*, Anaheim, CA, CD-ROM, March 2003.
9. Garofalo, F., Fundamentals of Creep and Creep-Rupture in Metals, MacMillian, NY, 1965.
10. Vianco, P. T., Private Communications.
11. Vianco, P. and J. Rejent, "Compression Deformation Response of 95.5Sn-3.9Ag-0.6Cu Solder," *UCLA lead-free workshop*, 2002.
12. Lau, J. H., S. Pan, and C. Chang, "Creep Analysis of Wafer Level Chip Scale Package (WLCSP) With 96.5Sn-3.5Ag and 100In Lead-Free Solder Joints and Microvia Build-Up Printed Circuit Board", *ASME Transactions, Journal of Electronic Packaging*, Vol. 124, 2002, pp. 69-76.
13. ANSYS, *User's Manual*, Release 6.1, 2002.
14. Cole, M., I. DeSousa, M. Interrante, J. Jozwiak, M. June, G. Martin, C. Milkovich, J. Ross, and M. Shannon, "The New Millennium for CCGA - Beyond 2000 I/O", *Proceedings of SMI*, Chicago, IL, 2001, pp. 297-306.
15. Lau, J. H., "Solder Joint Reliability of Flip Chip and Plastic Ball Grid Array Assemblies Under Thermal, Mechanical, and Vibration Conditions", *Proceedings of IEEE Japan International Electronics Manufacturing Technology Symposium*, 1995, pp. 13-19.
16. Lau, J. H., Z. Mei, S. Pang, C. Amsden, J. Rayner, and S. Pan, "Creep Analysis and Thermal-Fatigue Life Prediction of the Lead-Free Solder Sealing Ring of a Photonic Switch", *ASME Transactions, Journal of Electronic Packaging*, Vol. 124, 2002, pp. 403-410.